JOURNAL OF PROPULSION AND POWER
Vol. 26, No. 4, July–August 2010

Effects of Wavy Surface Roughness on the Performance of Micronozzles

Federico La Torre,* Sasa Kenjeres,† and Chris R. Kleijn‡
Delft University of Technology, 2628 BW Delft, The Netherlands
and
Jean-Luc P. A. Moerel§
TNO Defence, Security and Safety, 2280 AA Rijswijk, The Netherlands

DOI: 10.2514/1.44828

Recent trends in small-scale (∼1 dm^3) satellites motivate the further development of microscale propulsion subsystems. In the present paper, we focus on flow dynamics simulations of conical convergent–divergent micronozzles and on the increased importance of wall effects due to the decrease in the characteristic length of such small systems. The inefficiency associated with viscous losses due to the developing boundary layer and the effect of sinusoidal surface roughness due to the employed microelectromechanical-system fabrication techniques are studied through computational fluid dynamics simulations for nonturbulent, nonrarefied flow conditions. Depending on the specific nature of the surface roughness, the formation and reflection of several weak shocks and, as a consequence, a decreased performance are observed.

Nomenclature

A_e	=	nozzle exit cross-sectional area, m^2
A_t	=	nozzle throat cross-sectional area, m^2
D_e	=	nozzle outflow diameter, m
D_i	=	nozzle inlet diameter, m
D_t	=	nozzle throat diameter, m
Kn	=	Knudsen number based on throat diameter
M	=	Mach number
m	=	mass flow rate, kg/s
P_a	=	ambient pressure, Pa
P_e	=	exit pressure, Pa
P_0	=	inlet pressure, Pa
Re	=	Reynolds number based on throat diameter
R_c	=	nozzle curvature radius at the throat, m
R_t	=	nozzle throat radius, m
T_{ideal}	=	ideal thrust, N
T_{real}	=	real thrust, N
T_0	=	inlet temperature, K
X, Y	=	Cartesian coordinates, m
V_e	=	exit velocity, m/s
η	=	relative efficiency of the thruster
θ_1	=	nozzle convergent angle
θ_2	=	nozzle divergent angle

I. Introduction

VARIOUS trends in the spacecraft industry are driving the development of so-called microsatellites (which have a typical volume of 1 dm^3). Microspacecraft seem to meet the new directives required by the space industry: faster, better, and less expensive. Even though a microsatellite may contain only one instrument, the reduction in complexity may lead to lower overall costs by facilitating systems integration. In addition, the small size allows for the selection of a smaller, less expensive, launch vehicle or the launch of multiple satellites per vehicle. Small-scale, low-mass, low-thrust, microchannel-based propulsion systems are particularly suitable for achieving precise control and maneuverability of future-generation small spacecrafts and satellites. Typically, these propulsion systems are manufactured using techniques from microelectromechanical systems (MEMS) technology. Some aspects of the large multidisciplinary research program that are being carried out in the development of such propulsion systems are shown in [1–4].

The fluid dynamics of micropropulsion thrusters differ from conventional large-scale propulsion systems in three important aspects:

1) The surface-to-volume ratio is many orders of magnitude larger, as it scales with the inverse square root of the thrust.

2) The Reynolds number, which scales with the square root of the thrust, is orders of magnitude lower too (see Table 1).

3) The surface roughness is significant compared with typical nozzle dimensions (see Fig. 1).

Although nearly all supersonic nozzles that are currently used in spacecraft have been designed using mainly inviscid flow calculations, when going into the microscale ($Re \leq 10000$), viscosity effects can no longer be neglected. As a result, there are two main areas of concern with MEMS-based micronozzles: the inefficiency associated with viscous losses due to the developing boundary layer and the effect of surface roughness. Both of these effects lead to a different behavior of the flow and the growth of the boundary layer, so that the nonviscous core flow expands less than expected, with a consequent decrease of the nozzle's performance.

Micronozzle hydrodynamics have been studied through two-dimensional augmented Burnett equations [5] and through numerical computational fluid dynamics (CFD) simulations in, for example, [6–9]. For very small-scale nozzles, rarefaction effects start to play a role. This has been accounted for through the use of CFD with wall slip boundary conditions [10–14] and through the use of direct simulation Monte Carlo (DSMC) techniques [10,14–19]. For DSMC, an error analysis has also been conducted [20]. Some geometrical aspects such as the dimension of the throat [18], the shape of the divergent [21,22], and the three-dimensional shape of the nozzle [16,23] have been investigated, also observing the influence of viscous effects in relation to the inlet conditions [23]. Some comparisons between numerical data and measurements have been provided in [24,25]. Wall roughness effects for large-size

Received 9 April 2009; revision received 29 January 2010; accepted for publication 2 February 2010.

*Ph.D. Student, Faculty of Applied Sciences, Department of Multi Scale Physics; FLaTorre@tudelft.nl.

†Assistant Professor, Faculty of Applied Sciences, Department of Multi Scale Physics; S.Kenjeres@tudelft.nl.

‡Professor, Faculty of Applied Sciences, Department of Multi Scale Physics; C.R.Kleijn@tudelft.nl.

§Research Scientist, Department of System Performance and Survivability, P.O. Box 45; Jean-Luc.Moerel@tno.nl.

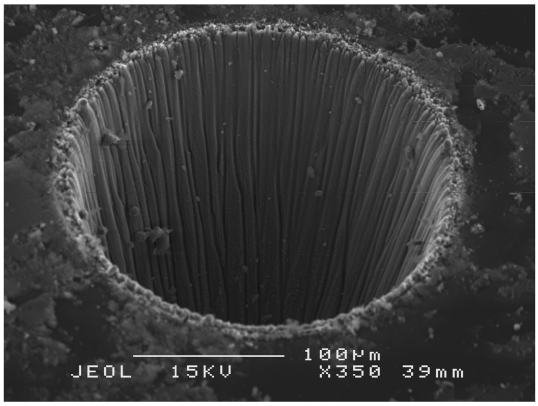

a)

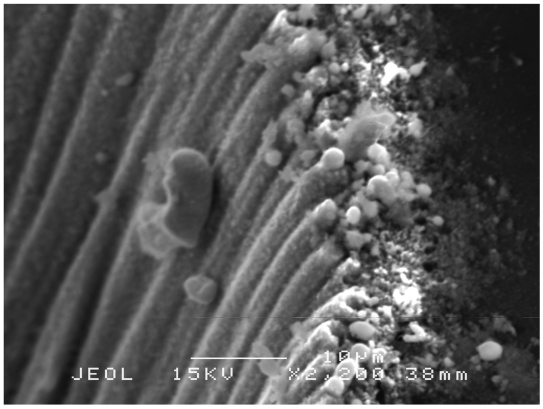

b)

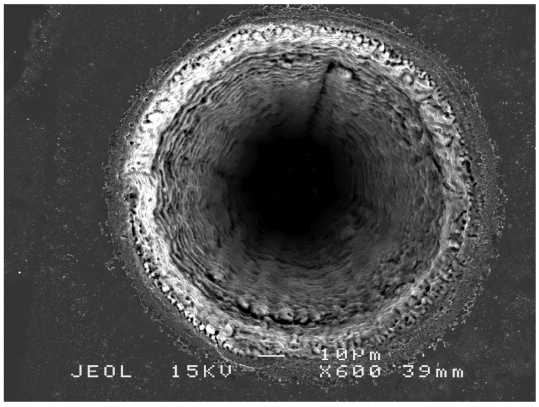

c)

Fig. 1 SEM images of the surface roughness in MEMS fabricated mN nozzles [2]: a) longitudinal wavy roughness patterns, b) a zoomed region, and c) transversal wavy roughness patterns.

nozzles and turbulent flow have been studied in [26]. The effect of wall roughness on the flow exhausting from micronozzles and impinging on rough surfaces was studied in [27], in which a regular triangular roughness inside the nozzle was found to lead to significant changes in the density field for configurations for which the subsonic region occupied a large part of the diverging nozzle. DSMC investigations of wall-roughness effects for micronozzles operating at low pressure (10^3–10^4 Pa), using different models to describe the way the particles impinge and reflect from the wall, were performed in [16,28]. Also using DSMC simulations, the influence of wall roughness, modeled as regular triangular and regular structures, on subsonic flows in microchannels was studied in [29].

In contrast to the above studies, the main objective of the present study is to discuss the effects of wall roughness on the low-Reynolds-number continuum supersonic flow in micronozzles, operated at stagnation pressures of several bars, and with wall roughnesses comparable to the characteristic (e.g., throat) dimensions of the nozzle.

In this paper, we focus on the influence of miniaturization on the performance of a particular nozzle design, especially with respect to the growth of the boundary layer and the influence of an irregular rough wall. After a brief discussion about our numerical approach to the problem (Sec. II) and an overview of the main aspects regarding the viscous losses due to the developing boundary layer for jets expanding into vacuum (Sec. III), we present our simulation results for micronozzles with a sinusoidal surface roughness (Sec. IV).

II. Numerical Approach

All the simulations presented in this paper have been run with the general-purpose CFD code FLUENT version 6.3 [30].

Three different regions can be distinguished in the studied geometry, as shown in Fig. 2: a straight inlet channel, which was taken into account in order to model the chamber and obtain the correct velocity profile at the inlet of the nozzle, a convergent part, in which the flow is accelerated from the initial subsonic velocity to the sonic condition (which is reached at the throat), and a divergent part, in which the flow supersonically expands to the outlet.

For most two-dimensional simulations, the curvilinear orthogonal grid, generated with Gambit [31], consists of quadrilateral elements, with 100 grid cells in the radial direction and about 600 grid cells in the axial direction. To study roughness effects, a finer or coarser grid has been used in order to meet accuracy requirements or to overcome computational limits, as will be explained later. The numerical mesh used for three-dimensional simulations will also be discussed later.

In the inlet we introduce nitrogen gas at a fixed pressure and temperature of, respectively, $P_0 = 10$ bar and $T_0 = 293$ K. The nitrogen gas is treated as an ideal gas, with temperature-dependent viscosity and thermal conductivity computed from kinetic theory. The walls of the nozzle are assumed to be adiabatic. Outside the nozzle outlet, a far-field pressure boundary condition $P_a = 0$ (vacuum) is imposed. As an initial guess for the solution, the nozzle exit pressure P_e was computed from the 1-D isentropic flow theory [32]. In the simulations, when the flow becomes supersonic, this specified nozzle exit pressure is no longer used as a boundary condition, but the exit pressure is extrapolated from the interior [30]. To check the influence of the used outflow boundary condition, we also performed simulations in which a large computational area was added downstream of the nozzle exit, and the far-field vacuum condition was imposed far downstream from the exit. For the configurations studied in this paper, no significant differences were observed between the two approaches. The nozzle inlet, throat, and outlet diameters are calculated for an ideal nonviscous nozzle of the given nominal thrust, whereas the actual thrust is an outcome of the simulations.

The solved equations include the continuity equation, the momentum balance (Navier–Stokes) equations in compressible form, and the thermal energy equation, all in steady-state formulation. These equations were discretized in space using a second-order upwind scheme and solved using FLUENT's implicit coupled solver. The accuracy of the numerical solution has been tested by comparing, for the same problem, results obtained with different discretization schemes (first-, second-, and third-order) and different meshes (double and quadruple times the number of cells in each direction). Negligible differences were observed between the presented results and those obtained with a third-order scheme on the finest mesh.

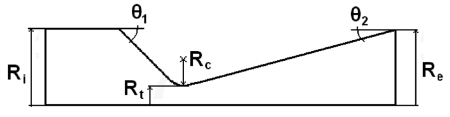

Fig. 2 Outline of the conical nozzle and its geometrical parameters used in the present study.

In Table 1, the Reynolds number, throat radius, and Knudsen number Kn (based on the throat radius) are reported for nozzles of varying nominal thrust. The results apply to an inlet of gaseous N_2 at 293 K and 10 bar, expelled through the nozzle vacuum. For nozzles with a thrust of ~0.1 mN or above, rarefaction effects are assumed to be negligible based on the low (less than 0.05) value of the Knudsen number. Although the Reynolds number of the flow in nozzles with a thrust larger than ~1 mN is sufficiently high to indicate that the flow may be turbulent, we assumed the flow for all studied thrusts to be laminar, and we did not include any turbulence modeling. In our preliminary studies we conclude that the application of different turbulence models, including also models with low-Reynolds-number wall corrections, was not able to produce and sustain any significant levels of turbulence. Even for the highest-Reynolds-number case considered (i.e., ~1 N thrust, $Re \sim 10^5$), the effective thrust with and without use of turbulence models did not produce any significant differences (i.e., less than 1.5% of difference obtained). We concluded that the flow through the nozzle remains laminar at these thrusts, even if there is a large boundary layer, probably because turbulence has neither time nor space to develop.

III. Viscous Effects

The presence of large viscous effects in the flow leads to the growth of the boundary layer; this means that the nonviscous core expands less than expected, causing a decreased nozzle performance. This effect becomes increasingly important for nozzles of decreasing thrust, i.e., decreasing dimensions. This is illustrated in Fig. 3, in which Mach number contours are plotted for nozzles with geometrical configuration: $\theta_1 = 45°$, $\theta_2 = 15°$, $R_c = R_t$, and with nominal (i.e., ideal nonviscous) thrusts decreasing from 1 N to 0.1 mN. It can be seen that for the smaller nozzles the outflow velocity is smaller than expected for an ideal nozzle in the absence of viscous effects. With the thrust T related to the exit velocity V_e through

$$T_{\text{real}} = \int_{\text{outlet area}} [mV_e + (p_e - p_a)]\, \mathrm{d}A \tag{1}$$

this leads to a decreased realized thrust T_{real} compared with the ideal thrust T_{ideal} for a nonviscous nozzle. Figure 4 further illustrates the increasing thickness of the boundary layer in the divergent for nozzles of various nominal thrust. Here, the boundary layer has been defined by the division line between the inviscid core and the region where the velocity is below 95% of the velocity at the centerline. In Table 2, the thickness of the boundary layer, as defined above, is reported for nozzles with nominal thrusts between 1 N and 1 mN at different locations along the divergent: $X/R_t = 0.028$, 0.057, 0.085, and 0.113. A dramatic increase of the boundary-layer thickness with decreasing nominal thrust is found: up to 30 and 50% of the outlet area for 1 and 0.1 mN micronozzles, respectively. If we define the relative efficiency η of a thruster (in this situation, almost similar to the efficiency of the nozzle) as

$$\eta = \frac{T_{\text{real}}}{T_{\text{ideal}}} \tag{2}$$

we find efficiencies of 98.0, 92.7, and 89.4% for the 1 N, 1 mN, and 0.1 mN nozzles, respectively, as shown in Fig. 3.

Table 1 Re, R_t, and Kn based on the throat radius for nozzles with an expansion ratio of 16 and nominal thrusts between 1 MN and 1 μN

Thrust, N	Re	R_t, m	Kn
10^6	1.3×10^8	4.3×10^{-1}	4.7×10^{-7}
10^3	4.1×10^6	1.4×10^{-2}	1.4×10^{-5}
10^0	1.3×10^5	4.3×10^{-4}	4.7×10^{-4}
10^{-3}	4.1×10^3	1.4×10^{-5}	1.4×10^{-2}
10^{-6}	1.3×10^2	4.3×10^{-7}	4.7×10^{-1}

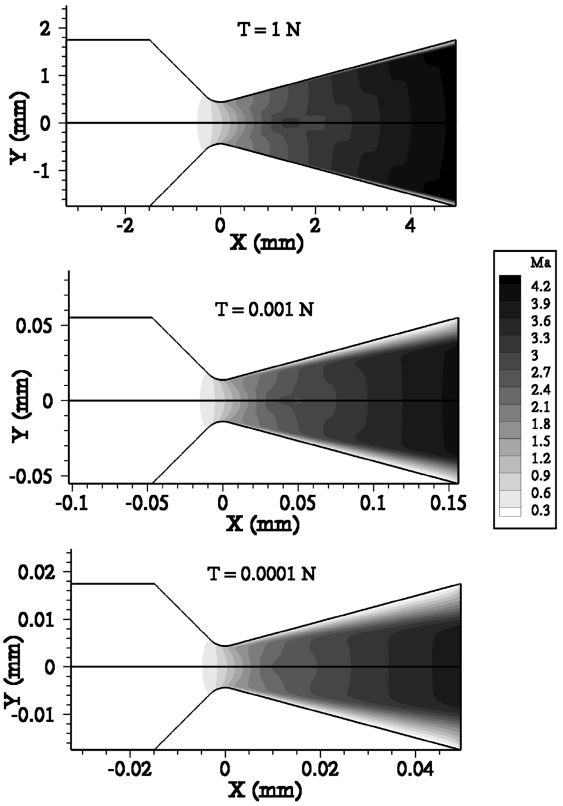

Fig. 3 Mach number contours for micronozzles of (nominally, i.e., for nonviscous flow) 1 N (upper), 1 mN (middle), and 0.1 mN (lower) thrust.

IV. Roughness Effects

Micronozzles are usually manufactured using MEMS technology, with which it is difficult to manufacture walls that are perfectly smooth relative to the small overall dimensions of the system. The nozzle assembly addressed in the present paper essentially consists of a silicon disc of ~7 mm diameter containing an array of small nozzles (micronozzles), bonded onto a glass tube for hermetic sealing. The nozzles in the silicon disc are manufactured using femtosecond laser machining by ultrashort laser pulses of a high

Table 2 Boundary-layer thickness relative to the local divergent radius at different locations along the divergent for nozzles with an expansion ratio of 16 and nominal thrusts between 1 N and 0.1 mN

	Boundary-layer thickness relative to local divergent radius, %			
Thrust, N	$X/R_t = 0.028$	$X/R_t = 0.057$	$X/R_t = 0.085$	$X/R_t = 0.113$
1	4.8	5.6	5.9	6.6
10^{-1}	7.1	9.3	11.7	12.3
10^{-2}	11.2	14.6	18.5	19.9
10^{-3}	18.8	23.4	29.0	32.4
10^{-4}	33.3	41.6	44.5	47.4

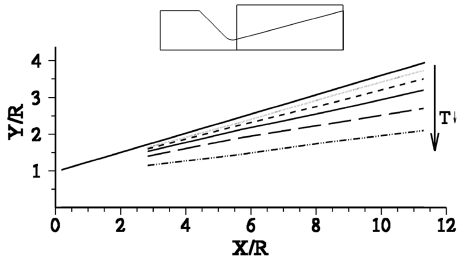

Fig. 4 Decrease of the effective nozzle expansion ratio A_e/A_t, due to the presence of a boundary layer (the bold lines indicate the outer wall and the symmetry axis of the nozzles).

energy content, thereby causing some of the material to ablate, resulting in good accuracy and repeatability, referring to the manufacturing limits of such dimensions (see Fig. 1) [2,33,34]. To obtain the conical-divergent nozzle shape, the silicon disc is machined from two sides. The slope of the nozzle side wall is controlled by the fluence of the laser spot; it has been shown that the slope of the nozzle wall depends on the pulse energy in the laser spot, machining speed, and pulse repetition rate on one hand and the threshold fluence for ablation on the other. It was observed from measurements that individual nozzles produced in this way differ from each other and from the specifications. Also, as expected, it was not possible to avoid the presence of rough bumps on the walls [2], which seem to be a residue of the micropillars that are formed on the silicon surface due to the laser treatment, as shown in Figs. 1a–1c and explained in [31]. In general, the final roughness strongly depends on the settings of the laser used for manufacturing, as explained in the general paper about laser ablation on solids [35].

For a nozzle with a nominal thrust $T_{\text{ideal}} = 1.14$ mN, $\theta_1 = 15°$, $\theta_2 = 15°$, and $R_c = 0$ μm, we studied the effect of a sinusoidal surface roughness with amplitudes varying between 2 and 4 μm (corresponding to 2–4% of the 50 μm throat diameter) and half-wavelengths varying between 2 and 10 μm (corresponding to 4–20% of the throat diameter), both in the longitudinal (i.e., parallel to the main flow) and in the azimuthal (i.e., perpendicular to the main flow) directions.

The choice of a sinusoidal surface roughness was based on a careful qualitative analysis of scanning electron microscope (SEM) images of the micronozzle [2], such as those displayed in Figs. 1. Depending on the settings during manufacturing, both longitudinal (Figs. 1a and 1b) and transversal (Fig. 1c) wavy structures can be observed on the nozzle walls. Unfortunately, a more quantitative analysis of the surface roughness, e.g., by performing profilometer measurements of the surface, was not feasible inside the conical micronozzle. The SEM images suggest that a sinusoidal roughness is better suited to reproduce the observed roughness than other models previously studied in literature, e.g., triangular or square roughness [27,29]. The images also suggest values of the amplitude and half-wavelength of the surface roughness that lie in the range stated above.

In the case of roughness in azimuthal direction, the flow is still 2-D-axisymmetric. Compared with the smooth-wall simulations presented above, a grid refinement has been applied to the two-dimensional grid in order to have at least eight cells in the axial direction within one half-wavelength. A zoom into the grid near the walls is displayed in Fig. 5.

For different azimuthal wall-roughness configurations, Table 3 lists the resulting thruster efficiency, Fig. 6 displays the Mach number contours, and Fig. 7a displays the same quantity along the axis of the nozzle. This kind of roughness was found to lead to a decreased performance: up to around 15%. The effective thrust decreases with increasing amplitude and decreasing half-wavelength of the surface roughness. The most obvious hypothesis to explain this performance decrease is an increase in friction and boundary-layer thickness. This, however, was observed only for small half-wavelengths (Fig. 6a), whereas wall roughnesses with larger half-wavelengths were found to lead to an interesting behavior of the flow along the divergent part of the nozzle. In this case, depending on the specific geometry of the surface roughness, the formation and reflection of several weak shocks was observed, due to the alternating relative increase and decrease in nozzle cross-sectional area (Fig. 6b). In addition to reducing the velocity magnitude and causing a loss of total pressure, these shocks (Fig. 7a) lead to a deviation of the flow direction from the axial direction. Since the thrust of the nozzle depends only on the axial component of the velocity, such a deviation causes a loss in efficiency.

To study the influence of the computational mesh on the observed shock structures and on the nozzle performance, a grid refinement study was performed for two particular geometries with rough walls. The results of this grid dependence study are listed in Table 4. Compared with the standard meshes, we halved, doubled, and quadrupled the number of grid points in each direction. The efficiencies predicted on the quadrupled meshes differ less than 0.3% from those predicted on the standard meshes. For the 10 μm roughness half-wavelength, the location of the first shock as predicted on the quadrupled mesh differs less than 0.1% from that predicted on the standard mesh. The predicted shock strength on the finest mesh differs less than 7% from that predicted on the standard mesh. The small difference between the predicted shock structures on various meshes is shown in Fig. 7b. For a roughness half-

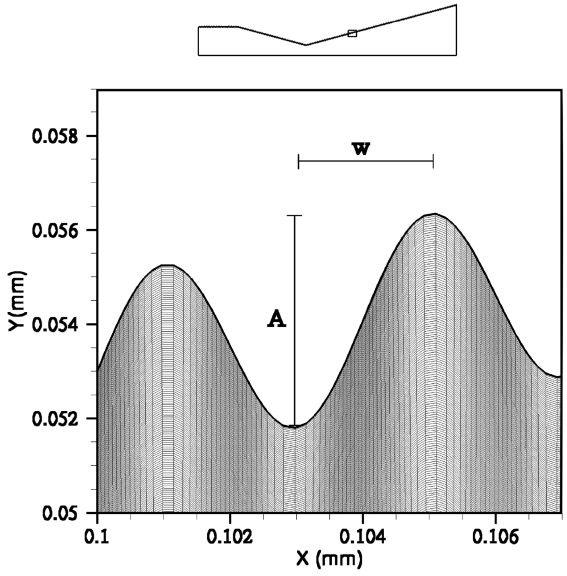

Fig. 5 A small part (see upper figure for the location on the nozzle wall) of the 5200 × 800 mesh used for the simulation of a nozzle with sinusoidal wall-roughness amplitude A of 4 μm and roughness half-wavelength w of 2 μm.

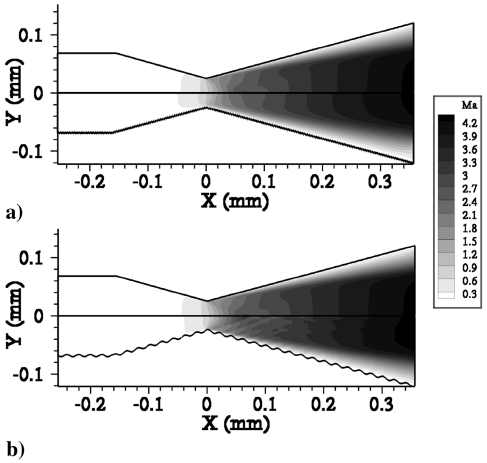

Fig. 6 Mach number contours for a 1.14 mN (nominal) micronozzle with smooth wall (top halves of both figures) and rough wall (bottom halves of both figures) with a) $w = 2$ μm and $A = 4$ μm and b) $w = 10$ μm and $A = 4$ μm.

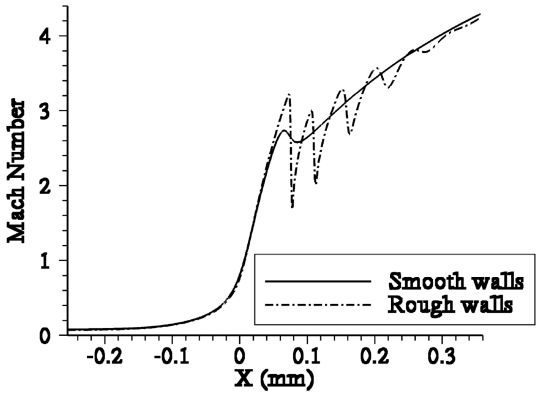

a)

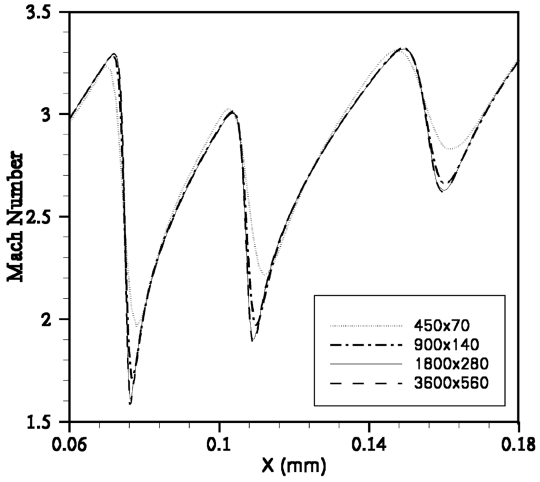

b)

Fig. 7 Mach number computed along the axis for a 1.14 mN (nominal) micronozzle: a) comparison between smooth wall and rough wall with half-wavelength of the sinusoidal roughness of 10 μm and amplitude of 4 μm and b) zoomed region of the divergent for the rough wall and different grid refinement.

wavelength of 2 μm, no shocks were detected on any of the used meshes.

A larger surface-roughness amplitude did not necessarily lead to a larger number of shocks, but it did lead to stronger shocks. Consequently, there were larger pressure losses and stronger deviations from the axial flow direction, leading to a further decrease in performance. This observation was further investigated by extending the range of the sinusoidal half-wavelengths up to 50 μm at a fixed amplitude of 4 μm and considering the number of shocks appearing in the divergent part of the nozzle and the position and strength of the first of these shocks as collected in the graph of Fig. 8. The following was found for larger half-wavelengths:

1) The weak shocks started to appear further downstream from the nozzle throat (Fig. 8b).

2) The number of these shocks was reduced (Fig. 8a).

Table 3 Thruster efficiency for different azimuthal wall-roughness configurations.

Roughness amplitude, μm	Roughness half-wavelength, μm	η, %
Smooth wall	——	92.39
4	2	75.21
4	6	78.11
4	10	78.62
2	2	83.77
2	10	85.41

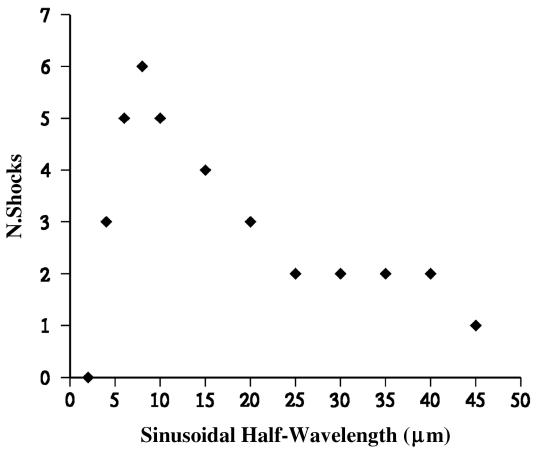

a)

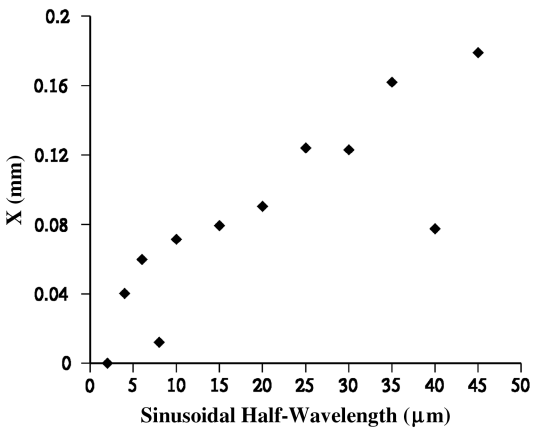

b)

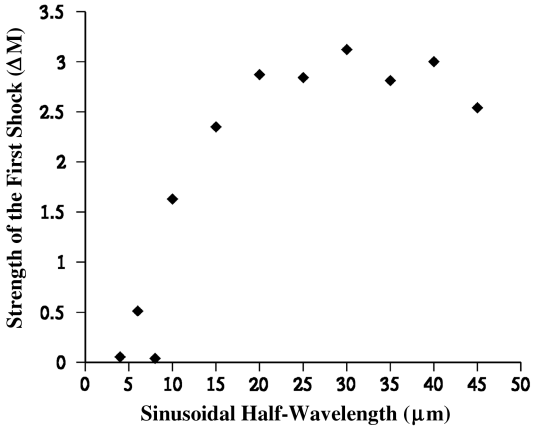

c)

Fig. 8 Effects of the sinusoidal half-wavelength on the a) number, b) position, and c) strength of the shocks in the divergent, for a wave amplitude of 4 μm.

3) The strength of the first shock increased, with a consequent degradation of the nozzle performance (Fig. 8c).

In Fig. 8a the case with the lowest half-wavelength was also reported, even if no shocks were observed in this configuration. Some anomalies in the general trend of the position of the first shock were detected for two configurations, in which the shock took place earlier than expected (Fig. 8b). The first of these two configurations corresponded to a very weak first shock (Fig. 8c). Looking at the flow pattern, Fig. 9 displays the velocity vectors field near the wall, inside the cavities, in which no significant flow recirculation was observed. On the other hand, as expected, a changes in the velocity have been observed in the core of the divergent nozzle, as shown in Fig. 10, in

Table 4 Relative efficiency, position, and strength of the first shock for different grid refinement for a 1.14 mN (nominal) micronozzle

Grid refinement	η, %	First shock position, m	First shock strength, ΔM
Roughness amplitude 4 μm, roughness half-wavelength 2 μm			
650 × 100	74.74	——	——
1300 × 200	75.21	——	——
2600 × 400	75.40	——	——
5200 × 800	75.52	——	——
Roughness amplitude 4 μm, roughness half-wavelength 10 μm			
450 × 70	77.86	6.99×10^{-5}	1.28
450 × 140	78.62	7.15×10^{-5}	1.63
900 × 280	78.85	7.14×10^{-5}	1.71
1800 × 520	78.82	7.14×10^{-5}	1.74

which a comparison of the velocity vectors for a nozzle with smooth and rough walls (sinusoidal half-wavelength of 10 μm and amplitude of 4 μm) in a zoomed region of the divergent part of the nozzle is displayed.

A different behavior was observed for a sinusoidal surface roughness parallel to the main flow direction. To simulate this situation, a three-dimensional geometry was modeled, representing one-quarter of the entire nozzle. The considered three-dimensional geometry filled with Mach number contours on the two planes of symmetry and at different cross sections is displayed in Fig. 11. Because of computational limitations, a coarser mesh had to be used here than for the previous two-dimensional simulations, with 250 grid cells in the axial direction, 50 grid cells in the radial direction, and 80 grid cells in the azimuthal direction. For this orientation of the surface roughness, no significant deviations in thrust were found compared with a smooth-wall nozzle, as can also be seen from the Mach number contours in Fig. 12. This can be explained from the fact that the flow mainly develops along the longitudinal direction and, in this case, does not experience alternating variations in the cross-sectional surface area.

At the end of this section we note that the observed decrease in effective thrust, compared with the ideal nonviscous thrust, as a

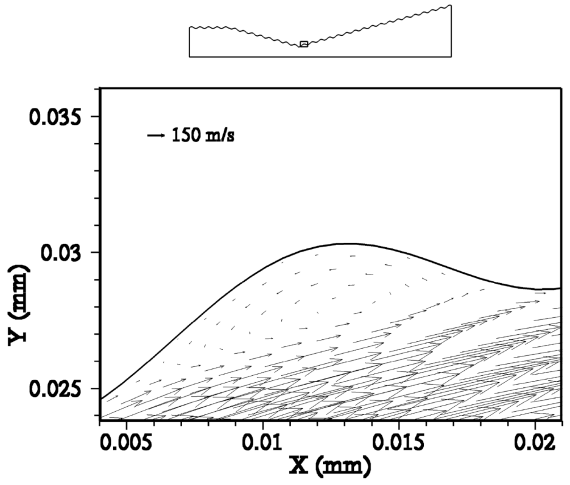

Fig. 9 Velocity vectors near the wall, in the region indicated by the rectangle in the upper picture.

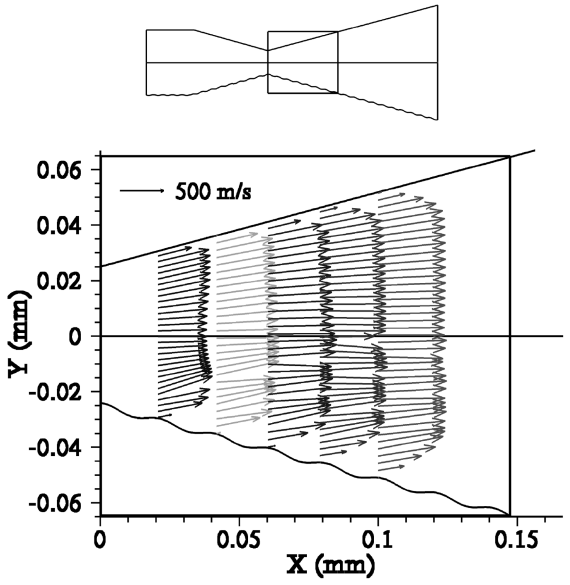

Fig. 10 Velocity vectors for a nozzle with smooth (upper) and rough (bottom) walls.

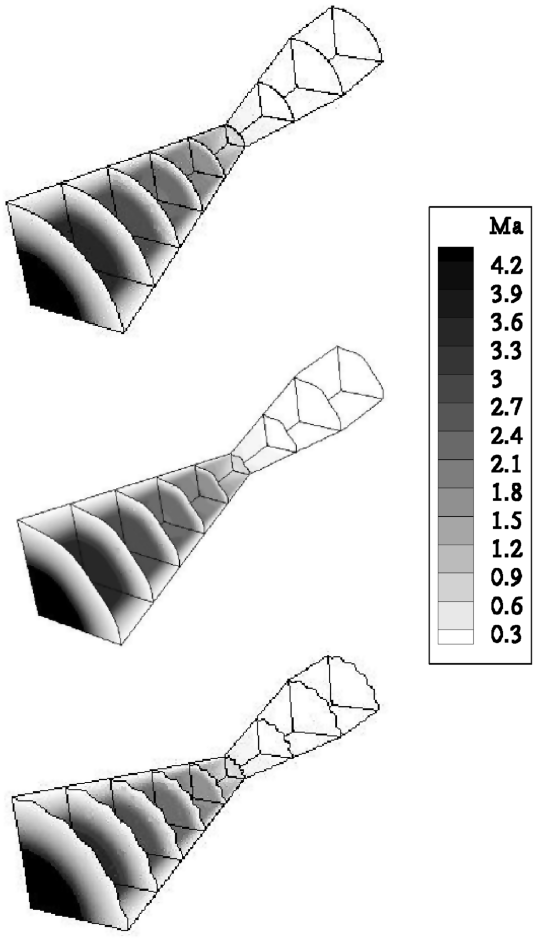

Fig. 11 Mach number contours on the two planes of symmetry and different cross sections for a 1 mN nozzle with no roughness (upper), large half-wavelength longitudinal roughness (center) and small half-wavelength longitudinal roughness (bottom).

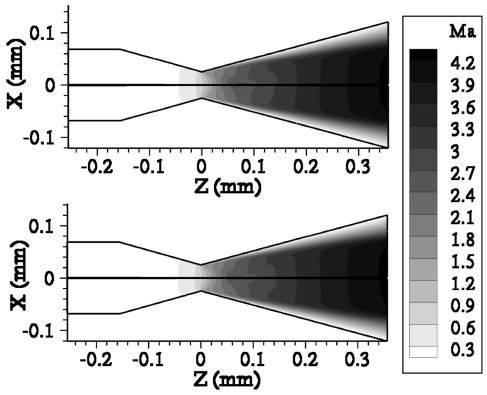

Fig. 12 Mach number contours (in the plane at an angle of 45° with the two planes of symmetry) for a $T_{\text{ideal}} = 1$ mN micronozzle with smooth wall (top halves of both figures) and rough wall in the longitudinal direction (bottom halves of both figures; $w = 2$ μm with $A = 4$ μm and $w = 10$ μm with $A = 4$ μm, respectively.

consequence of boundary-layer formation (section III) and surface roughness (section IV), is difficult to determine experimentally. On one hand, the relative effect of boundary layers and surface roughness is small and hard to measure in nozzles with large thrusts. On the other hand, in nozzles with small thrust, where the relative effect is significant, the total thrust is too small to be measured accurately. In a previous study [3], we have compared experimentally observed thrusts for a 25 mN atmospheric pressure nozzle with our numerical results and we have found that the simulations were in good agreement with experiments within experimental error.

V. Conclusions

It has been pointed out that cold-gas nitrogen micronozzles with thrusts of 1 mN and lower (operating typically at several bars of inlet pressure and expansion ratios of the order of 16) behave differently from what is commonly known for large-scale nozzles. The presence of strong viscous effects and the consequent growth of the boundary layer in the divergent part of the nozzle play an important role in the flow expansion and should be taken into account when designing efficient configurations and computing their thrust. The performance loss due to viscous effects is higher than 10% for nozzles with a nominal thrust below 1 mN.

Surface roughnesses with an amplitude of 2–4% of the throat diameter and an orientation perpendicular to the main flow direction were found to lead to the formation of multiple weak shocks along the divergent part of the nozzle and to performance reductions up to 18%. An increase in the surface-roughness half-wavelength led to the formation of a lower number of shocks with greater strength and a consequent further degradation of performances. Surface roughnesses oriented in the direction parallel to the flow were found not to significantly influence the flow and the thrust.

Acknowledgments

The project is funded by MicroNed, one of the Dutch Besluit Subsidies Investeringen Kennisinfrastructuur (BSIK) research programs. The authors wish to acknowledge the contribution of B. T. C Zandbergen (Delft University of Technology) for the useful discussions, and J. G. Louwerse (University Twente) for making available the scanning electron microscope images.

References

[1] Moerel, J. L. P. A., Sanders, H. M., Louwerse, M. C., Jansen, H. V., Boscher, J., Zandbergen, B. T. C., La Torre, F., Kenjeres, S., and Kleijn, C. R., "Development of Micro Propulsion System Technologies for Minisatellites in the Netherlands," 5th International Spacecraft Propulsion Conference, Paper 12, 2008.

[2] Zandbergen, B. T. C., Louwerse, M. C., Tardaguila, F., Koopmans, R. J., Boscher, J., and Moerel, J. L. P. A., "Initial Development of a Miniature Cold Gas Propulsion System for Nano/Microsatellites," 5th International Spacecraft Propulsion Conference, Paper 19, 2008.

[3] La Torre, F., Kenjeres, S., Kleijn, C. R., Moerel, J. L. P. A., and Zandbergen, B. T. C., "Influence of Boundary Layer Formation and Surface Roughness on the Thrust of Micronozzle," 5th International Spacecraft Propulsion Conference, Paper 18, 2008.

[4] Bradshaw, N., Moerel, J. L. P. A., and Sanders, H. M., "Critical Gasdynamic Aspects for Micro Nozzles," Faculty of Aerospace Engineering, Delft Univ. of Technology, Delft, The Netherlands, 2005.

[5] San, O., and Bayraktar, I., "Numerical Modeling of Gas Flow in Converging-Diverging Micronozzles," 37th Fluid Dynamics Conference and Exhibit, AIAA Paper 2007-3986, 2007.

[6] Xie, C., "Characteristics of Micronozzle Gas Flows," *Physics of Fluids*, Vol. 19, No. 3, 2007, Paper 037102. doi:10.1063/1.2709707

[7] Buoni, M., Kietz, D., Aslam, K., and Subramaniam, V. V., "Simulation of a Compressible Gas Flow in a Micronozzle," 35th AIAA Thermophysics Conference, AIAA Paper 2001-3073, 2001.

[8] Thornber, B., Chesta, E., Gloth, O., Brandt, R., Schwane, R., Perigo, D., and Smith, P., "Numerical Simulation of Micronozzles with Comparison to Experimental Results, 4th International Spacecraft Propulsion Conference, Paper 131, 2004.

[9] Chen, K., Winter, M., and Huang, R. F., "Supersonic Flow in Miniature Nozzles of the Planar Configuration," *Journal of Micromechanics and Microengineering*, Vol. 15, No. 9, 2005, pp. 1736–1744. doi:10.1088/0960-1317/15/9/016

[10] Liu, M., Zhang, X., Zhang, G., and Chen, Y., "Study on Micronozzle Flow and Propulsion Performance Using DSMC and Continuum Methods," *Acta Mechanica Sinica*, Vol. 22, No. 5, 2006, pp. 409–416. doi:10.1007/s10409-006-0020-y

[11] Markelov, G. N., Ivanov, M. S., Ketsdever, A. D., and Wadsworth, D. C., "Numerical Study of Cold Gas Micronozzle Flows," 33th Aerospace Science Meeting and Exhibit, AIAA Paper 99-0166, 1999.

[12] Raju, R., Pandey, B. P., and Roy, S., "Finite Element Model of Fluid Flow Inside a Microthruster," *NanoTech 2002 Conference*, AIAA Paper 2002-5733, 2002.

[13] Gadepalli, V. V. V., and Lin, C., "Navier-Stokes Modeling of Gas Flows in a De-Laval Micronozzle," 44th AIAA Aerospace Sciences Meeting and Exhibit, AIAA Paper 2006-1425, 2006.

[14] Titov, E., Gallagher-Rogers, A., and Levin, D., "Examination of a Collision-Limiter Direct Simulation Monte Carlo Method for Micropropulsion Applications," *Journal of Propulsion and Power*, Vol. 24, No. 2, 2008, pp. 311–321. doi:10.2514/1.28793

[15] Zelesnik, D., Micci, M., and Long, L., "Direct Simulation Monte Carlo Model of Low Reynolds Number Nozzle Flows," *Journal of Propulsion and Power*, Vol. 10, No. 4, 1994, pp. 546–553. doi:10.2514/3.23807

[16] Alexenko, A. A., Levin, D. A., Gimelschin, S. F., and Collins, R. J., "Numerical Modeling of Axisymmetric and Three-Dimensional Flows in MEMS Nozzle," *AIAA Journal*, Vol. 40, No. 5, 2002, pp. 897-904. doi:10.2514/2.1726

[17] Alexenko, A. A., Fedosov, D. A., Levin, D. A., Gimelschin, S. F., and Collins, R. J., "Performance Analysis of Microthrusters Based on Coupled Thermal-Fluid Modeling and Simulations," *Journal of Propulsion and Power*, Vol. 21, No. 1, 2005, pp. 95–101. doi:10.2514/1.5354

[18] Mo, H., Lin, C., Gokaltun, S., and P. V., Skudarnov, "Numerical Study of Axisymmetric Gas Flow in Conical Micronozzle by DSMC and Continuum Methods," 44th AIAA Aerospace Sciences Meeting and Exhibit, AIAA Paper 2006-991, 2006.

[19] Stein, W. B., and Alexenko, A. A., "Application of the DSMC Method for Design of a Coaxial Microthruster Nozzle," 44th Joint Propulsion Conference & Exhibit, AIAA Paper 2008-4530, 2008.

[20] Titov, E., and Levin, D., "Analyses of Numerical Errors in the Kinetic Modeling of Microthruster Devices," *Journal of Thermophysics and Heat Transfer*, Vol. 21, No. 3, 2007, pp. 616–622. doi:10.2514/1.28737

[21] Engblom, W. A., O'Gara, M., Richards, A., and Sypeck, D. J., "Investigation of Microthruster Nozzle Performance for Nanosatellite Applications," 37th AIAA Fluid Dynamic Conference and Exhibit, AIAA Paper 2007-3985, 2007.

[22] Louisos, W. F., and Hitt, D. L., "Viscous Effects on the Performance of Two-Dimensional Supersonic Linear Micronozzles," *Journal of Spacecraft and Rockets*, Vol. 45, No. 4, 2008, pp. 706–715. doi:10.2514/1.33434

[23] Wang, M. R., and Li, Z. X., "Numerical Simulations on Performance of MEMS-Based Nozzle at Moderate Temperatures," *Microfluidics and Nanofluidics*, Vol. 1, No. 1, 2004, pp. 62–70.

doi:10.1007/s10404-004-0008.5
[24] Nagai, H., Naraoka, R., Sawada, K., and Asai, K., "Pressure-Sensitive Paint Measurement of Pressure Distribution in a Supersonic Micronozzle." *AIAA Journal*, Vol. 46, No. 1, 2008, pp. 215–222. doi:10.2514/1.28371
[25] Hao, P., Ding, Y., Yao, Z., He, F., and Zhu, K., "Size Effect on Gas Flow in Micro Nozzles," *Journal of Micromechanics and Microengineering*, Vol. 15, No. 11, 2005, pp. 2069–2073. doi:10.1088/0960-1317/15/11/011
[26] Krishnamurty, V. S., and Shyy, W., "Effect of Wall Roughness on the Flow Through Converging-Diverging Nozzles," *Journal of Propulsion and Power*, Vol. 13, No. 6, 1997, pp. 753–762. doi:10.2514/2.5248
[27] Ngalande, N., Lilly, T., Killingsworth, M., and Gimelshein, S., "Nozzle Plume Impingement on Spacecraft Surfaces: Effects of Surface Roughness," *Journal of Spacecraft and Rockets*, Vol. 43, No. 5, 2006, pp. 1013–1018. doi:10.2514/1.19321
[28] Ketsdever, A. D., Clabough, M. T., Gimelshein, S. F., and Alexeenko, A., "Experimental and Numerical Determination of Micropropulsion Device Efficiencies at Low-Reynolds Numbers," *AIAA Journal*, Vol. 43, No. 3, 2005, pp. 633–641. doi:10.2514/1.10284
[29] Lilly, T. C., Duncan, J. A., Nothnagel, S. L., Gimelshein, S. F., Gimelshein, N. E., Ketsdever, A. D., and Wysong, I. J., "Numerical and Experimental Investigation of Microchannel Flows with Rough Surfaces," *Physics of Fluids*, Vol. 19, 2007. doi:10.1063/1.2775977
[30] *FLUENT 6 Tutorial Guide*, FLUENT Inc., Natick, MA, 2005.
[31] *Gambit 2 Tutorial Guide*, FLUENT Inc., Natick, MA, 2001.
[32] Sutton, G. P., and Biblarz, O., *Rocket Propulsion Elements*, Wiley, New York, 2001.
[33] Louwerse, M. C., Jansen, H. V., Groenendijk, M. N. W., and Elwenspoek, M. C., "Nozzle Fabrication for Micropropulsion of a Microsatellite," *Journal of Micromechanics and Microengineering*, Vol. 19, No. 4, 2009, Paper 045008. doi:10.1088/0960-1317/19/4/045008
[34] Groenendijk, M. N. W., and Meijer, J., "Microstructuring Using Femtosecond Pulsed Laser Ablation," *Journal of Laser Applications*, Vol. 18, No. 3, 2006, pp. 227–235. doi:10.2351/1.2227020
[35] Chichkov, B. N., Momma, C., Nolte, S., von Alvensleben, F., and Tunnermann, A., "Femtosecond, Picosecond and Nanosecond Laser Ablation of Solids," *Journal of Applied Physics*, Vol. 63, 1996, pp. 109–115.

D. Talley
Editor-in-Chief